Published in final edited form as:

ACS Appl Bio Mater. 2024 May 20; 7(5): 3041–3049. doi:10.1021/acsabm.4c00080.

Hydrophilic Coating Microstructure Mediates Acute Drug Transfer in Drug-Coated Balloon Therapy

Tarek Shazly,
Department of Biomedical Engineering Program, College of Engineering and Computing, Department of Mechanical Engineering, College of Engineering and Computing, and Cardiovascular Translational Research Center, University of South Carolina, Columbia, South Carolina 29208, United States

John F. Eberth,
Biomedical Engineering, Science and Health Systems, Drexel University, Philadelphia, Pennsylvania 19104, United States

Colton J. Kostelnik,
Biomedical Engineering, Science and Health Systems, Drexel University, Philadelphia, Pennsylvania 19104, United States; Aerospace Engineering and Engineering Mechanics, The University of Texas at Austin, Austin, Texas 78712, United States

Mark J. Uline,
Department of Biomedical Engineering Program, College of Engineering and Computing, Cardiovascular Translational Research Center, and Department of Chemical Engineering, College of Engineering and Computing, University of South Carolina, Columbia, South Carolina 29208, United States

Vipul C. Chitalia,
Department of Medicine, Boston University School of Medicine, Boston, Massachusetts 02118, United States; VA Coston Healthcare System, Boston, Massachusetts 02115, United States

Francis G. Spinale,
Department of Biomedical Engineering Program, College of Engineering and Computing, Cardiovascular Translational Research Center, and Department of Cell Biology and Anatomy, School of Medicine, University of South Carolina, Columbia, South Carolina 29208, United States

Ahmed Alshareef,
Department of Biomedical Engineering Program, College of Engineering and Computing, Department of Mechanical Engineering, College of Engineering and Computing, and Cardiovascular Translational Research Center, University of South Carolina, Columbia, South Carolina 29208, United States

Vijaya B. Kolachalama

Corresponding Author: **Tarek Shazly** – *Department of Biomedical Engineering Program, College of Engineering and Computing, Department of Mechanical Engineering, College of Engineering and Computing, and Cardiovascular Translational Research Center, University of South Carolina, Columbia, South Carolina 29208, United States;* shazly@mailbox.sc.edu.

The authors declare no competing financial interest.

Department of Medicine, Boston University School of Medicine, Boston, Massachusetts 02118, United States; Department of Computer Science and Faculty of Computing & Data Sciences, Boston University, Boston, Massachusetts 02115, United States

Abstract

Drug-coated balloon (DCB) therapy is a promising endovascular treatment for obstructive arterial disease. The goal of DCB therapy is restoration of lumen patency in a stenotic vessel, whereby balloon deployment both mechanically compresses the offending lesion and locally delivers an antiproliferative drug, most commonly paclitaxel (PTX) or derivative compounds, to the arterial wall. Favorable long-term outcomes of DCB therapy thus require predictable and adequate PTX delivery, a process facilitated by coating excipients that promotes rapid drug transfer during the inflation period. While a variety of excipients have been considered in DCB design, there is a lack of understanding about the coating-specific biophysical determinants of essential device function, namely, acute drug transfer. We consider two hydrophilic excipients for PTX delivery, urea (UR) and poly(ethylene glycol) (PEG), and examine how compositional and preparational variables in the balloon surface spray-coating process impact resultant coating microstructure and in turn acute PTX transfer to the arterial wall. Specifically, we use scanning electron image analyses to quantify how coating microstructure is altered by excipient solid content and balloon-to-nozzle spray distance during the coating procedure and correlate obtained microstructural descriptors of coating aggregation to the efficiency of acute PTX transfer in a one-dimensional ex vivo model of DCB deployment. Experimental results suggest that despite the qualitatively different coating surface microstructures and apparent PTX transfer mechanisms exhibited with these excipients, the drug delivery efficiency is generally enhanced by coating aggregation on the balloon surface. We illustrate this microstructure–function relation with a finite element-based computational model of DCB deployment, which along with our experimental findings suggests a general design principle to increase drug delivery efficiency across a broad range of DCB designs.

Graphical Abstract

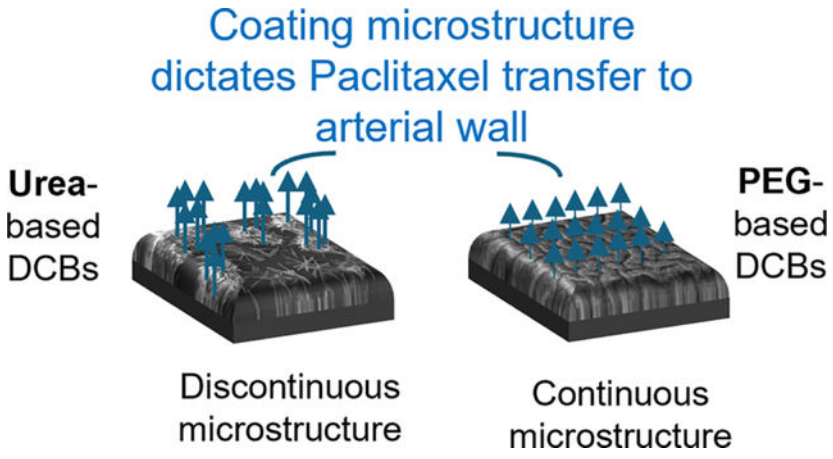

Keywords

drug-coated balloon; excipient; paclitaxel; coating microstructure; urea; polyethylene glycol

1. INTRODUCTION

Drug-coated balloon (DCB) therapy is an established treatment for peripheral artery disease (PAD), wherein balloon inflation in combination with the local delivery of the drug paclitaxel (PTX) or derivative compounds restores and retains lumen patency.[1–3] PTX is the leading antirestenotic drug in endovascular therapy due to its lipophilic properties, binding characteristics, and efficacy in preventing cellular proliferation at nanomolar tissue concentrations.[4] DCB enthusiasm can be attributed to the embodied leave-nothing-behind strategy, where in contrast to permanent implants such as bare-metal and drug-eluting stents, the potential exists for complete healing and restoration of the arterial milieu.[5] DCB therapy may include a preliminary address of the lesion site via various physical approaches (i.e., noncompliant intravascular balloon inflation, high-speed rotational atherectomy) but is centered around a transient (~2–3 min) balloon inflation that both further compresses the lesion and locally delivers drug to the arterial wall.[6–11] Thus, with no permanent implant, DCB therapy has the potential to acutely restore (via lesion dissection and mechanical compression) and subsequently maintain (via antiproliferative effects of PTX on resident cells) vessel patency, with no apparent restriction on the treated vessel size or initial plaque burden.

Despite large-scale clinical adoption of DCBs in PAD therapy, their comparatively sparse use in the coronary circulation suggests that clinical potential has not been fully realized.[12,13] Clinical hesitation for broader DCB use is in part due to our incomplete understanding of the key determinants of therapeutic efficacy[14–17] and the associated lack of generalizable strategies to promote efficient component transfer from the device to the arterial wall. Comparative studies among current devices indicate that only a small fraction of coating material (<10%) is transferred to and resorbed by the arterial wall and most of the initial PTX dose (>90%) is lost to systemic circulation—this leads to ineffective and unpredictable patient outcomes and increases the risk of off-target drug effects.[6,17,18]

Previous studies have aimed to enhance intraprocedural drug transfer via consideration of numerous balloon/coating designs, where typical device specification includes balloon size/compliance, drug type/dose, and excipient type/concentration.[19–22] A variety of excipients have been proposed in DCB design, including urea, polyethylene glycol, shellac/shelloic acid, polysorbate, dextran, and other proprietary materials.[4,23] In all cases, excipients play the vital role of promoting adequate tissue uptake/retention of PTX and thus potentiate localized therapy. A meta-analysis of excipient performance in DCBs suggests a notable trade-off between hydrophilic and hydrophobic materials: hydrophilic materials lead to higher tissue levels of PTX, while hydrophobic materials better resist drug wash-off during procedures.[24–27] Thus, hydrophilic excipients enhance the local delivery of PTX, which is a poorly water-soluble drug, but also increase the risk of premature systemic release. To mitigate this, DCBs are often sheathed until just before inflation (i.e., during catheter steering/balloon placement) to ensure proper drug deployment.

Given that PTX delivery is a primary function of DCBs, hydrophilic excipients have gained favor among device manufacturers despite the wash-off potential, with the remaining design imperative to increase drug delivery efficiency within this device subclass.[14,28–30]

In the present study, we seek to elucidate if the PTX delivery efficiency from DCBs formed with two leading hydrophilic excipients can be quantitatively related to the coating microstructure. Our focus on PTX transfer efficiency, as opposed to the total amount delivered, is in line with the notion that a higher fractional payload delivery will enable effective devices with a lower initial dosing, thus mitigating the risk of local tissue toxicity and off-target drug effects. Specifically, we consider PTX coating variants formed with the canonical excipients urea (UR) and polyethylene glycol (PEG) and examine how the titration of key compositional and preparational variables impacts both acute PTX delivery and defined metrics of the coating microstructure. The selection of UR and PEG as excipients in our study is reflective of currently approved devices (i.e., *IN.PACT Admiral*, Medtronic Vascular and *Stellarex*, Phillips), in which both enhanced intraprocedural drug delivery and potential for sustained delivery via coating uptake have been reported in clinical trials.[31–33] Our experimental findings indicate that increased coating aggregation, which can be achieved via an increased excipient solid content in the coating formulation or balloon-to-nozzle spray distance in the coating procedure, promotes acute PTX transfer from the coating to the arterial wall. Thus, despite the diverse microstructures and different modes of PTX transfer exhibited by these coatings, increased aggregation may represent a general strategy to enhance PTX delivery efficiency across a broad range of hydrophilic excipients. We illustrate this plausible microstructure–function relation with a finite element-based computational model of DCB deployment, with results from parametric studies that confirm the positive association between coating aggregation and PTX transfer.

2. METHODS

We performed an integrated set of experimental studies to establish correlations between hydrophilic excipient-based PTX coating microstructures and acute PTX transfer to arterial tissue in an ex vivo model of DCB deployment. We focused on two prototypical excipients for PTX delivery (UR and PEG) with nominally diverse microstructures upon spray-based surface coating and created coating variants via titration of compositional (excipient solid content) or preparational (spraying distance from surface) variables. Resultant coating microstructure was assessed via scanning electron microscopy (SEM) and quantitative image analyses, while acute PTX transfer was measured via liquid chromatography–mass spectrometry (LC-MS) on femoral artery samples following ex vivo coating-tissue contact studies that mimic DCB deployment. Deterministic microstructure–function relations identified ex vivo were then illustrated with a finite element-based computational model of DCB deployment.

2.1. Coating Synthesis.

Coating variants were formed using a spray-coating technique reflective of typical DCB preparational protocols.[34] Briefly, components were mixed with the appropriate solvents, namely ethanol (200 proof) for PTX (LC Laboratories, MA) and UR (Sigma-Aldrich) and a 5% aqueous solution of sodium bicarbonate for PEG (Sigma-Aldrich), homogenized via agitation (~200 rpm), and transferred to the payload cylinder of a spray-coater (Autolock, model no. PQ-30S). PTX alone or PTX + excipient solutions (concentrations specified below) were then sprayed (from a fixed spraying distance, specified below)

onto flat Nylon-12 films (0.5 mm thickness, precleaned via sonication in an ethanol bath at 40 °C) that served as a balloon surface surrogate, resulting in complete coverage of a greater than 25 × 25 mm film surface region for all preparational variants. The spray-coater was equipped with a 0.4 mm diameter tip, set to deliver 30 PSI for fluid compression, and held at a specified distance from the film to promote repeatable coating formation. Immediately following the spray-coating procedure, samples were placed in a room-temperature desiccator with controlled humidity (<5%) for 6 h to evaporate all solvents. The samples were stored in the desiccator until subsequent testing to prevent rehydration.

2.2. Compositional and Preparational Coating Variants.

Three types of coatings were formed for PTX delivery: PTX alone, PTX-UR, and PTX-PEG. In all cases, a 15 mg/mL solution of PTX was used in the spray coating procedure. Excipient solutions were prepared with solid contents of 5, 10 or 15% (w/v). *Compositional variants* of PTX-UR and PTX-PEG were formed via equal volume mixing of constituent solutions and a spray distance (distance from the nozzle tip to the film surface) of 12.5 cm. *Preparational variants* of the intermediate compositional variant (i.e., 10% excipient solid content) for both PTX-UR and PTX-PEG were formed using spray distances of 7.5, 12.5, or 17.5 cm. Following desiccation of all sprayed surfaces (described above), a 25 mm × 25 mm film surface region was cut to form test elements for subsequent PTX transfer and imaging studies; calculated test element properties (based on variant PTX/excipient solution formulations and spray distance) for all compositional and preparational variants are given in Table 1.

2.3. Ex Vivo Model of DCB Deployment.

We leveraged a uniaxial compression testing system to provide an ex vivo model of DCB deployment, in which the intima of freshly harvested porcine femoral arteries (8–12 months old, 75–125 lbs., female American Yorkshire pigs) was subjected to sustained contact with coated test elements.[29,35] Briefly, an excised tissue sample (prepared as a flat, circular specimen) and a coating variant test element were mounted onto flat surfaces, immobilized within the mechanical testing system (Bose ElectroForce 5270), and positioned such that tissue/coating surfaces were opposed and parallel (Figure 1). To initiate testing, the associated system software (Enduratec) was programmed to bring surfaces into contact via a ramped system arm displacement (0.01 mm/s) until a compressive interfacial force of 3 N was reached. Automated load control was then used to maintain the compressive force for an additional 3 min dwell period reflective of typical DCB inflation times. Upon dwell period completion the mobile system arm was retracted (0.01 mm/sec), and both the tissue sample and test element were removed from the system, snap-frozen via submersion in liquid nitrogen, and stored at −80 °C for further analysis.

2.4. Quantification of PTX Transfer to Arterial Tissue.

The acute drug transfer during ex vivo tissue-coating contact studies was measured via LC-MS as previously described.[29] Briefly, PTX was extracted via tissue sample submersion in methanol and 0.1% acidic acid (v/v) with constant agitation, sonication (2× for 30 min, with 3 min vortex mixing between runs), centrifugation (5000 rpm for 10 min), and supernatant

isolation. The obtained supernatant was then diluted in methanol and analyzed via LC-MS, followed by use of PTX standard curves to quantify tissue drug content.[29] Measured PTX in each tissue sample was compared to the initial PTX dose within the respective test element (Table 1) to compute the PTX transfer efficiency for coating variants.

2.5. Imaging and Quantification of Coating Surface Microstructure.

The surface microstructures of all coating variants formed with UR and PEG excipients were assessed via SEM. Following test element preparation (Section 2.1), samples were sputter coated (2.5 kV, 20 mA) with gold–palladium nanoparticles to provide an ~7.5 nm conductive layer over the native surface. SEM images were acquired at two magnification levels (400× and 1400×), enabling assessment of both qualitative structural differences between coating types and definition/quantification of coating-specific microstructural features. To quantify changes in coating microstructure following PTX transfer, additional SEM was conducted with intermediate variants formed with either excipient (10% solid content; 12.5 cm spraying distance) before and after tissue-coating contact studies.

All obtained SEM images were analyzed using custom code in MATLAB R2022b (MathWorks Inc., Natick, MA). Briefly, raw images were converted to grayscale and then corrected for nonuniform intensities by applying a bias field correction using multiplicative intrinsic component optimization (MICO).[36] The images were then binarized using a locally adaptive threshold with a sensitivity of 0.7. Lastly, the image was denoised using a minimum connected element threshold of 30 pixels (Figure 2). Measurements were computed on each image to quantify the microstructural features of the coating. Coating area fraction (c_{af}) for all images was defined as the percentage of the surface covered by coating, i.e., the fractional foreground content of the binarized images. Additional semiautomated measurements (ImageJ) were taken to quantify a coating aggregation index (c_{ag}), which represents the extent to which coating material accumulates in distinct microstructural domains as opposed to within a diffuse/uniform layer. For PTX-UR coatings, in which aggregate domains were typically circular with a characteristic diameter of ~15–30 μm and distinct from diffuse material domains, c_{ag} was defined as the number of aggregate domains per unit surface area. For PTX-PEG coatings, which formed comparatively continuous linear domains with a characteristic length of ~25–50 μm, identifiable regions between features enabled an automated definition of c_{ag} as the background content of binarized images (no material) per unit surface area. Both c_{af} and c_{ag} were computed with at least 20 measurements within 5 randomly selected subregions of a given image.

2.6. Finite Element-Based Model of DCB Drug Delivery.

A simple, 2D computational model of coating-arterial wall interaction was developed using a commercially available finite element-based multiphysics software (Comsol), with focus on the simulation of intraprocedural acute drug transfer to and transport within the arterial wall. The model geometry depicted an axial-radial cross-section of a femoral segment with two domains: the coating (C) and the arterial wall (A), wherein the former consisted of a series of semicircular, drug-containing aggregates uniformly distributed over a 50 mm length forming the tissue-coating interface, and the latter a pair of rectangular tissue domains spanning the tissue-DCB interface (50 mm length, 1 mm width). An initial 1 μM drug

concentration was assigned to all coating domains, reflecting typical dosing levels with current DCBs. Drug transport was modeled as diffusion-mediated within the aggregate domains, and diffusion-convection mediated within the arterial wall to account for interstitial flow. The effective drug diffusion coefficients (D) in either domain and interstitial flow velocity (v) in the arterial wall were estimated/assigned based on previously published values, namely $D_C = 1 \times 10^{-15}$ m^2/s, $D_A = 1 \times 10^{-12}$ m^2/s, and $v = 1 \times 0^{-8}$ m/s.[31–33] A no flux boundary condition was applied between the aggregate domains and underlying surface (i.e., the balloon); all other boundaries were assigned as open.

We defined the *aggregate domain number* as a geometric parameter in our simulation framework, which corresponds to the number of aggregate domains per 100 μm of interfacial length. Critically, variation in aggregate domain number (ranging from 1 to 8 in considered parametric studies) was coupled with variation in aggregate size/spacing such that the total drug content was constant across considered scenarios. A physics-controlled adaptive mesh utilizing a Delaney triangulation scheme was applied to the overall geometry (with an aggregate domain number of 8), and the governing transport equations were solved with a time-dependent solver over a 180 s period in 0.1 s increments. Solutions obtained with a total of 445 453 triangular elements were deemed mesh-independent based on a less than a 1% difference in coating drug content at 100 s with a further increase in mesh density; all subsequent simulations were conducted at or above this meshing density. Postprocessing of simulation data included surface integration of the drug concentration field in the C and A domains at all time points, which was then normalized by the initial drug content in the C domain.

2.7. Statistical Analyses.

Obtained experimental response variables are presented as mean and standard error values of N repeat measures. Statistical comparisons between experimental groups were determined using class I (fixed effects) analysis of variance (ANOVA) and an unpaired t test, with p-values <0.05 indicating significant differences. Simple linear regressions were performed between experimental response variables, where the Pearson's correlation coefficient R quantifies the strength of the relation.

3. RESULTS AND DISCUSSION

Obtained experimental results are presented and discussed in a manner that highlights the relationship between the hydrophilic coating microstructure and acute PTX transfer to arterial tissue in the context of DCBs. Using UR and PEG as canonical hydrophilic excipients for the PTX delivery, we synthesized a range of microstructurally diverse coating variants and identified a general determinant of acute drug transfer, namely, the degree of coating aggregation on the balloon surface. We provide complementary support for the potential utility of this coating design variable via computational simulation of DCB deployment, where obtained solutions illustrate the enhancement of intraprocedural arterial wall PTX concentration with increased coating aggregation.

3.1. Compositional Variation of UR and PEG Coatings.

PTX coatings formed with UR and PEG had qualitatively different coating microstructures, with PTX-UR characterized by needle-like constituents with distinct aggregation domains and PTX-PEG a comparatively continuous and textured surface. Progressive increase of either excipients' solid content caused evident changes in these characteristic features, including a tendency for increased constituent aggregation in PTX-UR and a progressive refinement of the surface texture in PTX-PEG (Figure 3A). With all but one of the considered compositional variants (*PTX-PEG, 5% excipient solid content*), PTX transfer was significantly increased in comparison to the *no excipient* condition, underscoring the need for this DCB component to facilitate adequate drug delivery (Figure 3B). At the highest examined excipient solid content (15%), PTX-UR and PTX-PEG exhibited respective 10-fold and 5-fold increases in PTX transfer efficiency as compared to the *no excipient* condition, underscoring the inherent capability of hydrophilic materials to promote rapid drug transfer to the arterial wall. Moreover, the 2-fold difference in PTX transfer efficiency with 15% UR versus 15% PEG suggests that the discontinuous and needle-like microstructure of the former enhances excipient-mediated drug delivery, a concept that has been experimentally observed and theoretically related to the tissue-coating contact pressure during inflation in our previous studies.[29,30]

3.2. Preparational Variation of UR and PEG Coatings.

Although PTX delivery efficiencies and surface imaging of compositional variants suggest a functional role of coating microstructure in the context of DCBs, these findings are potentially confounded by compositionally dependent alterations in coating compressibility and/or intracoating PTX transport kinetics operative during the inflation period. To further evaluate the potential role of the coating microstructure, analogous coating imaging/PTX transfer efficiency studies were conducted with preparational variants (with equivalent compositions) of PTX-UR and PTX-PEG. A comparison of obtained SEM images shows that increased spray distance causes an increase in apparent PTX-UR aggregation and refinement of PTX-PEG texture, qualitatively similar effects to increased excipient solid content (Figure 4A). Moreover, an increased spraying distance caused a monotonic increase in acute PTX transfer efficiency (Figure 4B), with significant differences between the closest and furthest spray distances for both PTX-UR (3-fold increase) and PTX-PEG (5-fold increase). Given that refinement of PTX-PEG texture corresponds with an increase in the aggregate number density, together these trends support the notion that microstructurally nonuniform coatings enhance PTX transfer with hydrophilic excipients.

3.3. Coating Microstructure and Apparent Drug Transfer Mechanisms.

Defined metrics obtained from SEM image processing (c_{af} and c_{ag}) exhibited monotonic changes with respect to compositional and preparational variations, suggesting that either variable can be used to effectively tune the coating microstructure in DCB design (Figure 5). Increasing the excipient solid content or spray distance in PTX-UR had no effect on c_{af} but caused dramatic increases in c_{ag}, indicating that these design variables enable alteration of the ratio between disperse and aggregate coating domains in a manner that retains continuity over the balloon surface (Figure 5A). In the case of PTX-PEG, induced changes in c_{af}

were again relatively minor, but there was a coupling with significant changes in c_{ag} in the examined variants (Figure 5B). These findings suggest that the induced reorganization of PTX-PEG coatings compacts material into aggregate domains, while reducing coating continuity over the balloon surface.

Comparison between intermediate coating variants (10% excipient solid content; 12.5 cm spray distance) before and after contact studies with arterial tissue indicates a different dominant mode of PTX transfer operative in PTX-UR and PTX-PEG. While simulated DCB deployment caused no apparent change in PTX-PEG microstructure, PTX-UR exhibited obvious differences resulting in a near total loss of aggregate domains (Figure 6A and B). Moreover, while c_{af} of PTX-PEG was unaffected by contact with tissue, PTX-UR was decrease by approximately 70% (Figure 6C). Taken together, these findings suggest that PTX-UR facilitates drug transfer via dissolution of aggregate domains upon hydration and contact with tissue, while PTX-PEG transfer is diffusion-mediated and occurs in the presence of a relatively stable coating microstructure.

3.4. Microstructure–Function Relations.

Positive correlations between c_{ag} and PTX transfer efficiency were found for both PTX-UR and PTX-PEG variants, suggesting that coating aggregation underlies a key microstructure–function relation in acute drug transfer (Figure 7). Interestingly, this notion applies to both coating types despite the noted difference in apparent drug transfer mode and thus may be applicable to a broad range of DCBs. We speculate that aggregation enhances PTX delivery by virtue of increasing the tissue-coating contact area per unit coating volume, which in PTX-UR accelerates aggregate domain tissue adsorption and in PTX-PEG promotes drug diffusion from the coating into the arterial wall. Our findings also suggest enhanced acute delivery with PTX-UR in comparison to PTX-PEG (Figure 3B vs 4B), which supports the previously identified advantage of a needle-like microstructure embodied by the former in terms of tissue-material mechanical interactions, including contact pressure with and penetration depth into the arterial wall.[30]

3.5. Illustrative Model of Aggregate-Mediated Drug Transfer.

Finite element-based computational modeling enabled isolation and quantification of the effect of coating aggregation on acute drug delivery in a 2-D simulation of DCB deployment (Figure 8A). The model considered drug transport via diffusion within the aggregate coating domains and diffusion-convection within the arterial wall. Given these considered transport mechanisms, the introduced aggregate domain number (aggregates formed from a fixed total coating volume, uniformly distributed over the tissue-balloon interface) and size together dictate the flux of drug into the arterial wall during the simulated inflation period. Simulation results indicate that the applied isometric increase in aggregate domain number significantly facilitates clearance of drug from the coating domains and consequently an increase in acute drug delivery to the arterial wall (Figure 8B and C). At the end of the 180 s inflation period, the highest considered aggregate domain number (8 aggregates per 100 μm DCB-tissue interface) resulted in complete drug clearance from the coating and approximately 60% of the initial dose transferred to the arterial wall, whereas with the lowest aggregate domain number (1 aggregate per 100 μm DCB–tissue interface),

approximately 30% of the drug remained in the coating and less than 40% of the initial dose was delivered to the arterial wall. The predicted effects of increased coating aggregation are in qualitative agreement with acute PTX transfer data obtained for both PTX-UR and PTX-PEG (Figure 7), supporting the use of this simplified framework to illustrate the role of coating microstructure in DCB delivery.

3.6. Study Limitations.

Our findings suggest that the microstructure of DCB coatings is a deterministic factor of PTX transfer efficiency during the balloon inflation period, wherein the aggregation of the coating on the balloon surface enhances drug delivery. Although we have developed this concept with microstructurally diverse hydrophilic excipients (UR and PEG) and coating variants formed via tuning of both compositional and preparational variables, several study limitations should be considered when interpreting and generalizing our results. First, our ex vivo model of DCB deployment (Section 2.3) is a 1-D mechanical loading of the tissue-coating interface and insomuch does not replicate the 2D mechanics of balloon inflation (if the process is modeled as the inflation of a thin-walled cylinder) and 3D tissue-coating contact mechanics. Moreover, our ex vivo studies do not account for the likely differences in coating microstructure pre- and post-inflation, probable changes in coating properties including hydrophilicity over the DCB shelf life,[37] the potential for altered coating biocompatibility due to aggregation, particularly the potential for particulate generation in the DCB context,[21] and only provide information on how coating aggregation just prior to/during tissue-coating contact impacts PTX transfer. Second, our ex vivo studies use healthy porcine femoral artery tissue, which will likely have different PTX transport properties from diseased human femoral arteries.[40] Despite this difference, we expect that the observed trends in coating variant delivery efficiencies will be qualitatively similar to those in a clinical setting. Third, we only examined a limited set of coatings (5 variants per excipient type) and thus do not have adequate data to fully establish the mechanistic relations underpinning altered PTX transfer despite obtained correlations with c_{ag} for both UR and PEG (Figure 7); moreover, these variants only deliver a single drug (PTX), although recent findings suggest the therapeutic benefit of codelivery of multiple drugs to further prevent postinterventional restenosis.[41] Finally, our illustrative computational model of DCB deployment (Section 2.6) ignores key biophysical factors that impact PTX retention/activity within the arterial wall, including binding/unbinding drug kinetics,[38,39] targeted tissue mechanical behavior[42] including modulation of the active response,[43] and only predicts total transient drug levels. Nevertheless, the general correspondence between model predictions and experimental data suggests that further refinement of transport process modeling and drug- and coating-specific parameter assignment can be used to guide DCB designs which seek to optimize coating microstructure.

4. CONCLUSIONS

Our study explored how DCB function is impacted by compositional and preparational manipulation of hydrophilic coating excipients, namely, UR and PEG. Our findings reveal that the microstructure of the coating, which is influenced by both excipient solid content and coating spray distance, plays a crucial role in acute PTX transfer to arterial

tissue. We observed that the increased aggregation of the coating on the balloon surface significantly boosts the PTX transfer efficiency. This enhancement is consistent across UR and PEG, despite their diverse microstructures and varied mechanisms of PTX transfer. Our computational simulations support these experimental observations, illustrating the importance of coating aggregation in improving drug delivery during DCB deployment. These results offer a new perspective on DCB design, emphasizing the need for a balanced approach that considers both the type of excipient used and the microstructural characteristics of the coating to maximize therapeutic efficacy in PAD treatment. This study paves the way for future research and development of DCB technologies, aiming to achieve more predictable outcomes in the management of obstructive arterial diseases.

ACKNOWLEDGMENTS

This project was supported by grants from the National Institutes of Health R01-HL159620, the American Heart Association (20SFRN35460031, 17SDG33670323), and SFRN 857078.

REFERENCES

(1). American Heart Association Statistics C. Heart Disease and Stroke Statistics-2017 Update: A Report From the American Heart Association. Circulation 2017, 135 (10), e146–e603. [PubMed: 28122885]

(2). McDermott MM; Kerwin DR; Liu K; Martin GJ; O'Brien E; Kaplan H; Greenland P Prevalence and significance of unrecognized lower extremity peripheral arterial disease in general medicine practice*. J. Gen Intern Med. 2001, 16 (6), 384–90. [PubMed: 11422635]

(3). Criqui MH; Aboyans V Epidemiology of peripheral artery disease. Circ. Res. 2015, 116 (9), 1509–26. [PubMed: 25908725]

(4). Torii S; Kolodgie FD; Virmani R; Finn AV IN.PACT Admiral drug-coated balloons in peripheral artery disease: current perspectives. Med. Devices (Auckl) 2019, 12, 53–64. [PubMed: 30858737]

(5). Bosiers M Leaving nothing behind. JACC Cardiovasc Interv. 2013, 6 (12), 1294. [PubMed: 24355119]

(6). Gray WA; Granada JF Drug-coated balloons for the prevention of vascular restenosis. Circulation. 2010, 121 (24), 2672–80. [PubMed: 20566965]

(7). Sarode K; Spelber DA; Bhatt DL; Mohammad A; Prasad A; Brilakis ES; Banerjee S Drug 7delivering technology for endovascular management of infrainguinal peripheral artery disease. JACC Cardiovasc Interv. 2014, 7 (8), 827–39. [PubMed: 25147028]

(8). Byrne R; Colleran R; Harada Y Drug coated balloon angioplasty in the treatment of peripheral arterial disease. Expert Rev. Med. Devices 2016, 13, 569–582. [PubMed: 27152654]

(9). Byrne RA; Joner M Drug-Coated Balloon Angioplasty for De Novo Stenosis: The Balloon is Back···Reloaded! JACC Cardiovasc Interv. 2015, 8 (15), 2010–2. [PubMed: 26627991]

(10). Byrne RA; Joner M; Alfonso F; Kastrati A Drug-coated balloon therapy in coronary and peripheral artery disease. Nat. Rev. Cardiol. 2014, 11 (1), 13–23. [PubMed: 24189405]

(11). Waksman R; Pakala R Drug-eluting balloon: the comeback kid? Circ Cardiovasc Interv. 2009, 2 (4), 352–358. [PubMed: 20031739]

(12). Loh JP; Waksman R Paclitaxel drug-coated balloons: a review of current status and emerging applications in native coronary artery de novo lesions. JACC Cardiovasc Interv. 2012, 5 (10), 1001–12. [PubMed: 23078727]

(13). Lazar FL; Onea HL; Olinic DM; Cortese BA 2024 scientific update on the clinical performance of drug-coated balloons. AsiaIntervention. 2024, 10 (1), 15–25. [PubMed: 38425817]

(14). Shazly T; Torres WM; Secemsky EA; Chitalia VC; Jaffer FA; Kolachalama VB Understudied factors in drug-coated balloon design and evaluation: A biophysical perspective. Bioeng Transl Med. 2023, 8 (1), No. e10370. [PubMed: 36684110]

(15). Bienek S; Kusmierczuk M; Schnorr B; Gemeinhardt O; Bettink S; Scheller B One single drug-coated balloon for all shapes/diameters? Neointimal proliferation inhibition in porcine peripheral arteries. PLoS One. 2023, 18 (1), No. e0280206. [PubMed: 36706120]

(16). Jun EJ; Shin ES; Kim B; Teoh EV; Chu CM; Kim S; Liew HB Coronary artery aneurysm formation after paclitaxel-coated balloon-only intervention for de novo coronary chronic total occlusion. Front Cardiovasc Med. 2023, 9, No. 1039316. [PubMed: 36684581]

(17). Cao Z; Li J; Fang Z; Feierkaiti Y; Zheng X; Jiang X The factors influencing the efficiency of drug-coated balloons. Front Cardiovasc Med. 2022, 9, No. 947776. [PubMed: 36312265]

(18). Herdeg C; Oberhoff M; Baumbach A; Blattner A; Axel DI; Schroder S; Heinle H; Karsch KR Local paclitaxel delivery for the prevention of restenosis: biological effects and efficacy in vivo. J. Am. Coll Cardiol. 2000, 35 (7), 1969–1976. [PubMed: 10841250]

(19). Cao Z; Li J; Fang Z; Feierkaiti Y; Zheng X; Jiang X The factors influencing the efficiency of drug-coated balloons. Front Cardiovasc Med. 2022, 9, No. 947776. [PubMed: 36312265]

(20). Marques L; Hopf-Jensen S; Preiss M; Mueller-Huelsbeck S An Update on Drug-eluting Technology in Peripheral Arteries to Treat Peripheral Arterial Disease. Heart Int. 2021, 15 (2), 73–78. [PubMed: 36277826]

(21). Xiong GM; Ang H; Lin J; Lui YS; Phua JL; Chan JN; Venkatraman S; Foin N; Huang Y Materials technology in drug eluting balloons: Current and future perspectives. J. Controlled Release 2016, 239 (239), 92–106.

(22). Speck U; Stolzenburg N; Peters D; Scheller B How does a drug-coated balloon work? Overview of coating techniques and their impact. J. Cardiovasc Surg (Torino). 2016, 57 (1), 3–11.

(23). Anbalakan K; Toh HW; Ang HY; Buist ML; Leo HL How does the Nature of an Excipient and an Atheroma Influence Drug-Coated Balloon Therapy? Cardiovasc Eng. Technol. 2022, 13 (6), 915–929. [PubMed: 35606568]

(24). Zhao B; Gu Z; Zhang Y; Li Z; Cheng L; Li C; Hong Y Starch-based carriers of paclitaxel: A systematic review of carriers, interactions, and mechanisms. Carbohydr. Polym. 2022, 291, No. 119628. [PubMed: 35698420]

(25). Anderson JA; Remund T; Pohlson K; Lamichhane S; Evans C; Evans R; Clark M; Egland K; Kelly P; Mani G In vitro and in vivo evaluation of effect of excipients in local delivery of paclitaxel using microporous infusion balloon catheters. J. Biomed Mater. Res. B Appl. Biomater. 2017, 105 (2), 376–390. [PubMed: 26513737]

(26). Anbalakan K; Toh HW; Ang HY; Buist ML; Leo HL How does the Nature of an Excipient and an Atheroma Influence Drug-Coated Balloon Therapy? Cardiovasc Eng. Technol. 2022, 13 (6), 915–929. [PubMed: 35606568]

(27). Cortese B; Kalkat H; Bathia G; Basavarajaiah S The evolution and revolution of drug coated balloons in coronary angioplasty: An up-to-date review of literature data. Catheter Cardiovasc Interv. 2023, 102 (6), 1069–1077. [PubMed: 37870079]

(28). Kitrou P; Katsanos K; Georgopoulou GA; Karnabatidis D Drug-Coated Balloons for the Dysfunctional Vascular Access: An Evidence-Based Road Map to Treatment and the Existing Obstacles. Semin Intervent Radiol. 2022, 39 (1), 56–65. [PubMed: 35210734]

(29). Azar D; Lott JT; Jabbarzadeh E; Shazly T; Kolachalama VB Surface Modification Using Ultraviolet-Ozone Treatment Enhances Acute Drug Transfer in Drug-Coated Balloon Therapy. Langmuir. 2020, 36 (17), 4645–4653. [PubMed: 32271583]

(30). Chang GH; Azar DA; Lyle C; Chitalia VC; Shazly T; Kolachalama VB Intrinsic coating morphology modulates acute drug transfer in drug-coated balloon therapy. Sci. Rep. 2019, 9 (1), 6839. [PubMed: 31048704]

(31). Peterson S; Hasenbank M; Silvestro C; Raina S IN.PACT Admiral drug-coated balloon: Durable, consistent and safe treatment for femoropopliteal peripheral artery disease. Adv. Drug Deliv Rev. 2017, 112, 69–77. [PubMed: 27771367]

(32). Tepe G; Zeller T; Albrecht T; Heller S; Schwarzwälder U; Beregi JP; Claussen CD; Oldenburg A; Scheller B; Speck U Local delivery of paclitaxel to inhibit restenosis during angioplasty of the leg. N Engl J. Med. 2008, 358 (7), 689–99. [PubMed: 18272892]

(33). Lyden SP; Faries PL; Niazi KAK; Sachar R; Jain A; Brodmann M; Werner M; Sood A; Krishnan P No Mortality Signal With Stellarex Low-Dose Paclitaxel DCB: ILLUMENATE Pivotal 4-Year Outcomes. J. Endovasc Ther. 2022, 29 (6), 929–936. [PubMed: 35000470]

(34). Turner EA; Atigh MK; Erwin MM; Christians U; Yazdani SK Coating and Pharmacokinetic Evaluation of Air Spray Coated Drug Coated Balloons. Cardiovasc. Eng. Technol. 2018, 9 (2), 240–250. [PubMed: 29497966]

(35). Zhou B; Ravindran S; Ferdous J; Kidane A; Sutton MA; Shazly T Using Digital Image Correlation to Characterize Local Strains on Vascular Tissue Specimens. J. Vis Exp. 2016, 107, No. e53625.

(36). Li C; Gore JC; Davatzikos C Multiplicative intrinsic component optimization (MICO) for MRI bias field estimation and tissue segmentation. Magn Reson Imaging. 2014, 32 (7), 913–23. [PubMed: 24928302]

(37). Rawat N; Benčina M; Paul D; Kovač J; Lakota K; Žigon P; Kralj-Iglič V; Ho HC; Vukomanović M; Iglič A; Junkar I Fine-Tuning the Nanostructured Titanium Oxide Surface for Selective Biological Response. ACS Appl. Bio Mater. 2023, 6 (12), 5481–5492.

(38). Creel CJ; Lovich MA; Edelman ER Arterial paclitaxel distribution and deposition. Circ. Res. 2000, 86 (8), 879–84. [PubMed: 10785510]

(39). Mandal PK; Sarifuddin; Kolachalama VB. Computational Model of Drug-Coated Balloon Delivery in a Patient-Specific Arterial Vessel with Heterogeneous Tissue Composition. Cardiovasc Eng. Technol. 2016, 7 (4), 406–419. [PubMed: 27443840]

(40). Kolachalama VB; Pacetti SD; Franses JW; Stankus JJ; Zhao HQ; Shazly T; Nikanorov A; Schwartz LB; Tzafriri AR; Edelman ER Mechanisms of tissue uptake and retention in zotarolimus-coated balloon therapy. Circulation. 2013, 127 (20), 2047–55. [PubMed: 23584359]

(41). Shazly T; Uline M; Webb C; Pederson B; Eberth JF; Kolachalama VB Novel Payloads to Mitigate Maladaptive Inward Arterial Remodeling in Drug-Coated Balloon Therapy. J. Biomech Eng. 2023, 145 (12), 121004. [PubMed: 37542712]

(42). Prim DA; Mohamed MA; Lane BA; Poblete K; Wierzbicki MA; Lessner SM; Shazly T; Eberth JF Comparative mechanics of diverse mammalian carotid arteries. PLoS One. 2018, 13 (8), No. e0202123. [PubMed: 30096185]

(43). Zhou B; Prim DA; Romito EJ; McNamara LP; Spinale FG; Shazly T; Eberth JF Contractile Smooth Muscle and Active Stress Generation in Porcine Common Carotids. J. Biomech Eng. 2018, 140 (1), 0145011. [PubMed: 28975258]

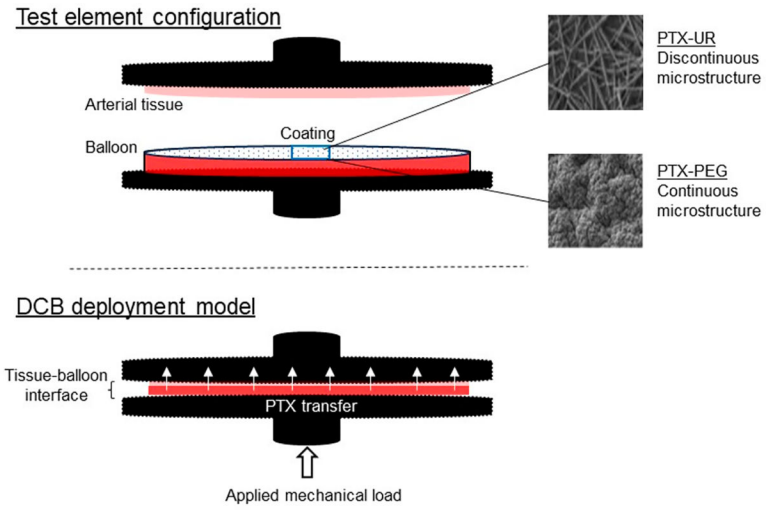

Figure 1.

Schematic of ex vivo model of DCB deployment. Controlled uniaxial loading of parallel test elements was used to initiate and sustain tissue-coating contact; a compressive mechanical load was sustained for 180 s, over which PTX was transferred from the coating to the arterial wall.

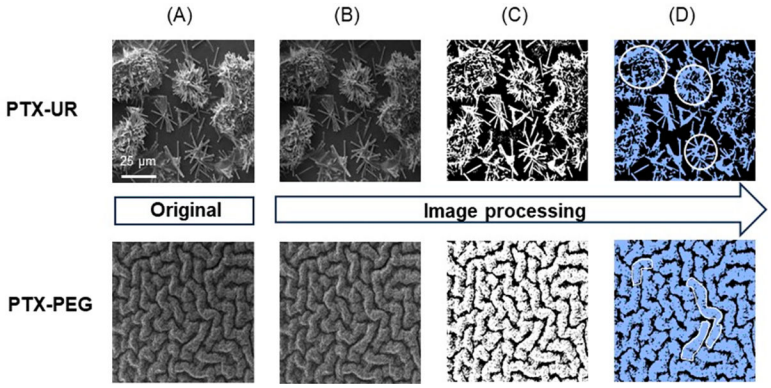

Figure 2.

SEM image processing. (A) SEM images of PTX-UR (top) and PTX-PEG (bottom) variants were used to characterize coating microstructure. Image processing[29] was applied to all original images by first (B) removing nonuniform intensities and applying a bias field correction via MICO, (C) followed by image binarization and locally adaptive thresholding, and finally (D) image denoising via a minimum connected element thresholding and local hole filling.

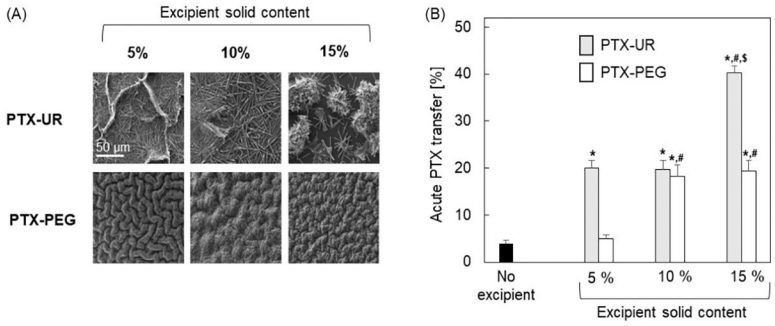

Figure 3.

Compositional variants of PTX-UR and PTX-PEG. (A) SEM images of PTX coatings formed with increasing excipient solid content: PTX-UR (top row) and PTX-PEG (bottom row). Coating surface morphologies depend on excipient, wherein PTX-urea coatings are discontinuous with discrete material domains and PTX-PEG coatings are comparatively continuous with wavy surface structure and evident texture. (B) Acute PTX transfer to arterial tissue following simulated DCB deployment. Both PTX-UR and PTX-PEG coatings exhibited increased drug transfer in comparison to the *no excipient* group, with increased excipient concentration generally enhancing drug transfer. Spray distance of 12.5 cm was used for the *no excipient* condition as well as all PTX-UR and PTX-PEG variants. Error bars represent SEM with $N = 6$. * indicates $p < 0.05$ vs PTX alone; # indicates $p < 0.05$ vs 5% variant of the respective excipient type; $ indicates $p < 0.05$ vs 10% variant of the respective excipient type.

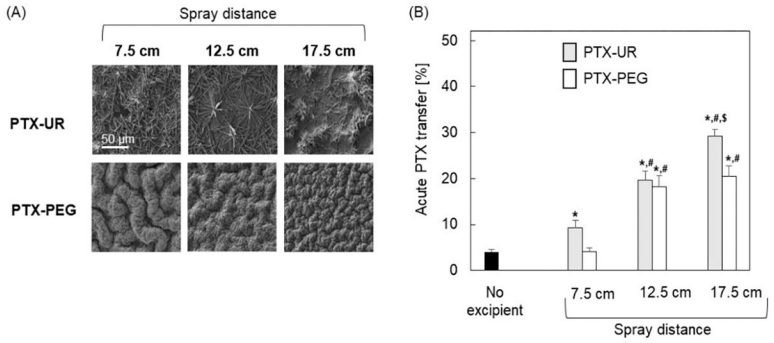

Figure 4.

Preparational variants of PTX-UR and PTX-PEG. (A) SEM images of PTX coatings formed with increasing spray distance during coating preparation: PTX-UR (top row) and PTX-PEG (bottom row). Morphological differences were observed among preparational variants, where increasing spray distance qualitatively increased material aggregation and refined surface texture in PTX-UR and PTX-PEG coatings, respectively. (B) Acute PTX transfer to arterial tissue in ex vivo model of DCB deployment. Both PTX-UR and PTX-PEG coatings exhibited increased drug transfer in comparison to the *no excipient* group, with increased spray distance promoting drug transfer. An excipient solid content of 10% was used for all PTX-UR and PTX-PEG variants. Error bars represent SEM with $N = 6$. * indicates $p < 0.05$ vs PTX alone; # indicates $p < 0.05$ vs 7.5 cm variant of the respective excipient type; $ indicates $p < 0.05$ vs 12.5 cm variant of the respective excipient type.

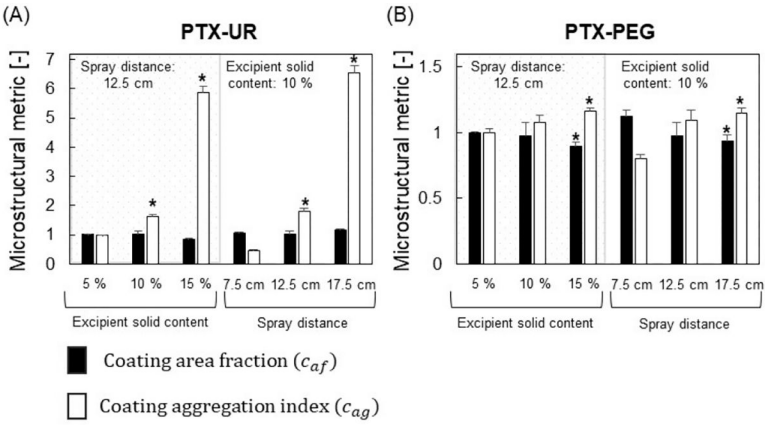

Figure 5.

Quantification of coating microstructure. Processed SEM images were used to quantify characteristic microstructural features. Coating area fraction (c_{af}) and an index of coating aggregation (c_{ag}) were computed for (A) PTX-UR and (B) PTX-PEG variants, presented as normalized values with respect to a selected coating variant (5% solid content; 7.5 cm spray distance) for each excipient type. Error bars represent SEM with $N = 6$. *indicates $p < 0.05$ vs selected coating variant (5% solid content; 7.5 cm spray distance) for each excipient type.

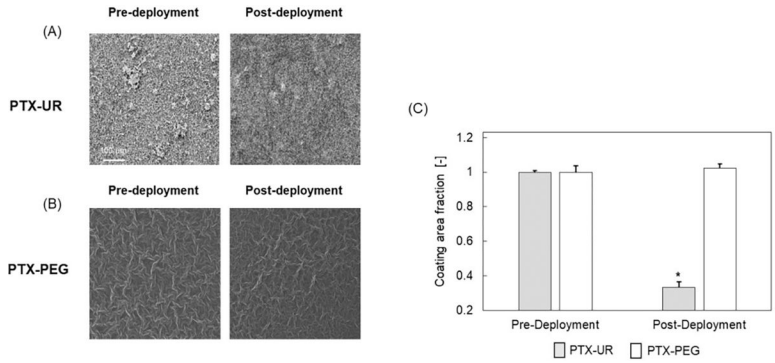

Figure 6.

Coating transfer during simulated balloon deployment. SEM images of (A) PTX-UR and (B) PTX-PEG coatings before and after interaction with arterial tissue in an ex vivo model of DCB deployment. Postdeployment, PTX-UR exhibited an apparent change in surface morphology characterized by a virtual absence of aggregate domains; conversely, PTX-PEG coatings exhibited no appreciable change in surface morphology. (C) Pre- and post-deployment coating area fractions for select PTX-UR and PTX-PEG variants (10% excipient solid content; 12.5 cm spray distance, with post-deployment values normalized with respect to the pre-deployment value for each coating. Error bars represent SEM with $N = 5$. *indicates $p < 0.05$ vs predeployment value for the respective coating type.

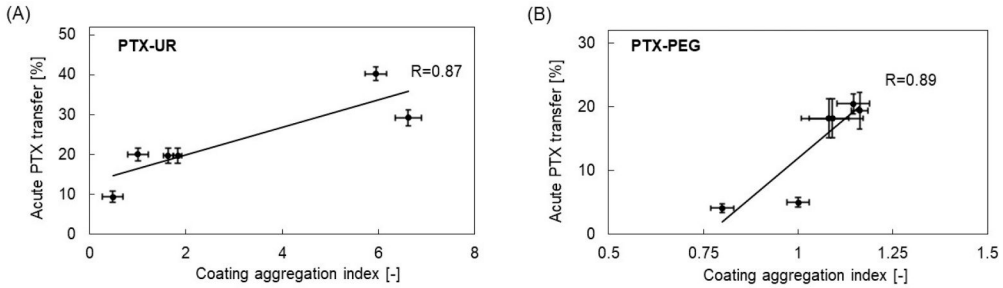

Figure 7.

Microstructure–function relations. Correlation between acute PTX transfer and the defined index of coating aggregation (c_{ag}) for (A) PTX-UR and (B) PTX-PEG variants. Strong positive correlations for both excipient types suggest that coating aggregation promotes drug transfer to arterial tissue in an ex vivo model of DCB deployment.

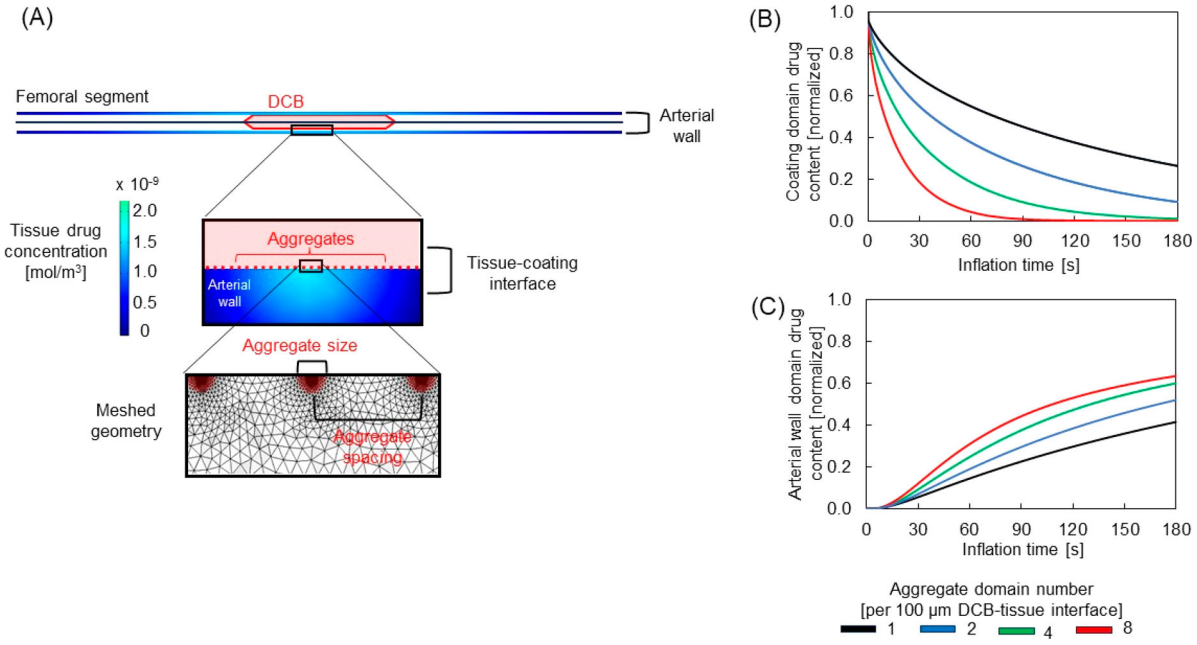

Figure 8.

Finite element-based computational model of DCB deployment. (A) A schematic depicting the modeled contact between the femoral artery and inflated DCB, which considered the spacing/size of aggregate domains in the DCB coating and provided predictions for the transient drug concentrations in the coating and arterial wall. Simulation predictions indicate that increased coating aggregation progressively increases (B) the release rate of drug from the coating and (C) the delivery rate of drug to the arterial wall over the 180 s inflation period.

Table 1.

Description of Compositional and Preparational Coating Variants[a]

Group	Composition/preparational variables		Test element properties		
	Excipient solid content (%)	Spray distance (cm)	Coating volume (μL)	PTX dose (μg)	PTX concentration (μg/mm^2)
Control (PTX alone)	0	12.5	N/A	200	0.32
Compositional Variants	5	12.5	1.0	200	0.32
	10	12.5	1.0	200	0.32
	15	12.5	1.0	200	0.32
Preparational Variants	10	7.5	1.7	345	0.55
	10	12.5	1.0	200	0.32
	10	17.5	0.7	133	0.21

[a] *Compositional variants* were formed by alteration of excipient solid content; *preparational variants* were formed by alteration of spray distance during the coating procedure. Calculated test element properties describe the coating volume and PTX dosing for all PTX-UR and PTX-PEG variants.